

DESIGN FABRICATION, AND INITIAL CHARACTERIZATION OF A 13 kW_e
METAL-HALIDE AND XENON SHORT-ARC LAMP HIGH-FLUX SOLAR
SIMULATOR WITH ADJUSTABLE CONCENTRATION PROFILES USING A
HORIZONTALLY-TRANSLATING CENTRAL LAMP

Thesis

Submitted to

The School of Engineering of the

UNIVERSITY OF DAYTON

In Partial Fulfillment of the Requirements for

The Degree of

Master of Science in Mechanical Engineering

By

Alexander Vence Ferreira

UNIVERSITY OF DAYTON

Dayton, Ohio

August 2023

DESIGN FABRICATION, AND INITIAL CHARACTERIZATION OF A 13 kW_e
METAL-HALIDE AND XENON SHORT-ARC LAMP HIGH-FLUX SOLAR
SIMULATOR WITH ADJUSTABLE CONCENTRATION PROFILES USING A
HORIZONTALLY-TRANSLATING CENTRAL LAMP

Name: Ferreira, Alexander Vence

APPROVED BY:

Andrew J. Schrader, Ph.D.
Advisory Committee Chairman
Professor
Mechanical & Aerospace Engineering

Rydge Mulford, Ph.D.
Committee Member
Professor
Mechanical & Aerospace Engineering

Hagan Evan Bush, Ph.D.
Committee Member
R&D, S&E Mechanical Engineering
Sandia National Labs

Robert Gill
Committee Member
Professor
Mercer University School of
Engineering

© Copyright by

Alexander Vence Ferreira

All rights reserved

2023

ABSTRACT

DESIGN FABRICATION, AND INITIAL CHARACTERIZATION OF A 13 kW_e METAL-HALIDE AND XENON SHORT-ARC LAMP HIGH-FLUX SOLAR SIMULATOR WITH ADJUSTABLE CONCENTRATION PROFILES USING A HORIZONTALLY-TRANSLATING CENTRAL LAMP

Name: Ferreira, Alexander Vence
University of Dayton
Advisor: Dr. Andrew J. Schrader

A novel, low cost, high flux solar simulator has been designed and built for the University to be able to undergo research on systems that need testing under high temperature solar irradiation. This simulator will feature four 2500W metal halide bulbs focused with elliptical reflectors, as well as one horizontally translating central 3000W Xenon short-arc lamp with a parabolic reflector and a convex lens acting as a secondary concentrator. To aid in the design, alignment, and characterization of the simulator a detailed Monte Carlo Ray Tracing suite has been developed. These models show that the simulator can produce a flux of 4.5kW/m² or around 4500 suns.

Dedicated to my parents

ACKNOWLEDGMENTS

I would like to thank my advisor Dr. Andrew J Schrader. He provided me with the equipment, space, and time to be able to do this work presented here. I would also like to thank him and Dr. Rydge Mulford for their work creating the Dayton Thermal Applications Lab on campus. It has truly been a dream come true to work with so many hard working, intelligent, and charismatic individuals in this collaborative environment.

I would also like to express my appreciation to everyone who has helped me with this work. Aaron Spieles, Natalie Douglass, Steven Ivec, and Jacob Brenner for offering their assistance whenever needed when building these systems. I would also like to thank Paul Rabinovits from strong lighting for offering his feedback on my designs.

TABLE OF CONTENTS

ABSTRACT.....	3
DEDICATION.....	4
ACKNOWLEDGMENTS	5
LIST OF FIGURES	8
LIST OF TABLES	11
LIST OF ABBREVIATIONS AND NOTATIONS.....	12
CHAPTER I INTRODUCTION.....	13
1.1 Motivation.....	13
1.2 Objectives	15
1.3 Thesis Overview	16
CHAPTER II LITERATURE REVIEW	18
2.1 Review of Other Simulators.....	18
2.2 Metal Halide Vs. Xenon Lamps.....	20
2.3 Primary and Secondary Concentrators.....	22
CHAPTER III MONTE CARLO RAY TRACING.....	24
3.1 Surface Emission	25
3.2 Tracing	28
3.3 Absorption, Reflection	29

3.4 Ray tracing through Participating media	29
CHAPTER IV INDIVIDUAL LAMP HOUSINGS	32
4.1 Design of Metal Halide Housing	32
4.2 Monte Carlo of Metal Halide Housing	35
4.3 Design of Xenon Lamp Housing	37
4.4 Monte Carlo Ray Tracing of Xenon Housing	41
4.5 Lamp Module Modeling Results	44
CHAPTER V FULL SIMULATOR.....	47
5.1 Design of Full Simulator.....	47
5.2 Monte Carlo Ray Tracing of Full Simulator	51
CHAPTER VI CONCLUSION AND FUTURE WORKS	56
REFERENCES	57

LIST OF FIGURES

<p>Figure 1.1: Contour map of solar resources in the United States However, effectively harnessing the United States’ solar resources is not without significant challenges as solar irradiation is dilute, unequally distributed, and intermittent.....</p> <p>Figure 1.2: Schematics of the principal solar concentrating technologies: (a) parabolic trough system, (b) tower system, and (c) a paraboloidal dish system with the rays from the sun representing reflection paths from the mirrors.</p> <p>Figure 1.3: Noor Concentrated Solar Power Plant in Morocco</p> <p>Figure 2.1: Simulators with flux aperture adjustments.....</p> <p>Figure 2.2: Metal-Halide (top) and xenon arc (bottom) lamps</p> <p>Figure 2.3: Spectral distribution of sunlight, xenon arc lamp, and metal halide lamp with Irradiance and relative spectral energy distribution on the Y axis and Wavelength on the x axis</p> <p>Figure 3.1: visualization of a single ray leaving a point.....</p> <p>Figure 3.2: Visualization of angles ϕ and θ.....</p> <p>Figure 3.3: Reflection and refraction at the interface between two optical media with different refractive indices.</p> <p>Figure 3.4: Philips MSR Gold 2.5kW FastFit metal halide lamp.....</p> <p>Figure 3.5: Optiforms E813 reflector with a 32 inch focal length a front diameter of 15 inches and a back diameter of 3 inches.....</p> <p>Figure 3.6: Reflectivity vs. wavelength of optiforms reflective silver coating</p> <p>Figure 4.1: Metal Halide lamp housing</p> <p>Figure 4.2: Arc model of metal halide lamp, it is a series of 9 nested ellipses</p>	<p>13</p> <p>14</p> <p>14</p> <p>19</p> <p>20</p> <p>21</p> <p>25</p> <p>27</p> <p>30</p> <p>32</p> <p>33</p> <p>33</p> <p>34</p> <p>35</p>
---	---

Figure 4.3: Specular reflection off an ellipsoidal reflector; u is the incoming ray r is the reflected ray and n is normal vector.....	37
Figure 4.4: Philips LTI 3kW-HS Standard Xenon Lamp with the cathode end on right and anode end on left.....	38
Figure 4.5: Xenon lamp support assembly from strong lighting with focus bearing assembly for small lamp adjustments	40
Figure 4.6: Xenon housing placed on pedestal with linear actuator for horizontal translation.....	40
Figure 4.7: Xenon arc model consisting of cylinder and sphere at the end	41
Figure 4.8: MCRT model of rays as they reflect off of the ellipsoidal reflector and make way towards the concentrating lens	42
Figure 4.9: Flux map of metal halide module generated with MCRT	44
Figure 4.10: Xenon module generated with MCRT.....	45
Figure 4.11: Plot of the number of rays vs peak flux and power in focal point.....	45
Figure 4.12: Plots showing effect of translating the xenon module	46
Figure 5.1: Rendering of 13kW high flux solar simulator.....	47
Figure 5.2: Side profile render of simulator with lamps pulled back	48
Figure 5.3: Adjustable platform and linear stage for metal halide housing allowing for 3 degrees of motion.....	49
Figure 5.4: Laser alignment procedure for top lamp	50
Figure 5.5: Laser point holders of single lamp angled to point at reflectors focal point. .	50
Figure 5.6: laser pointers placed on all 4 metal halide housing for alignment	51
Figure 5.7: First lamp configuration and flux map.....	52

Figure 5.8: second lamp configuration and flux map	53
Figure 5.9: Third lamp configuration and flux map	54
Figure 5.10: Flux map of full 5 lamp simulator.....	54
Figure 5.11: Flux maps at different positions in front and behind the focal plane	55

LIST OF TABLES

Table 2.1: A review of notable simulators and some of their important features. Notably the lamp type, the concentrator shape, the peak flux, and the spot.....	17
Table 2.2: Cost analysis of xenon vs metal halide lamps.....	18
Table 4.1: Reflectors and view factors	17

LIST OF ABBREVIATIONS AND NOTATIONS

CSP	Concentrated Solar Power
HFSS	High Flux Solar Simulator
MCRT	Monte Carlo Ray Tracing

CHAPTER I

INTRODUCTION

1.1 Motivation

As the world's climate crisis continues to unfold the emphasis on finding new sources of renewable energy has increased. Figure 1.1 shows a map of the solar resources across the United States' and the significant resource potential that exists in the American Southwest.

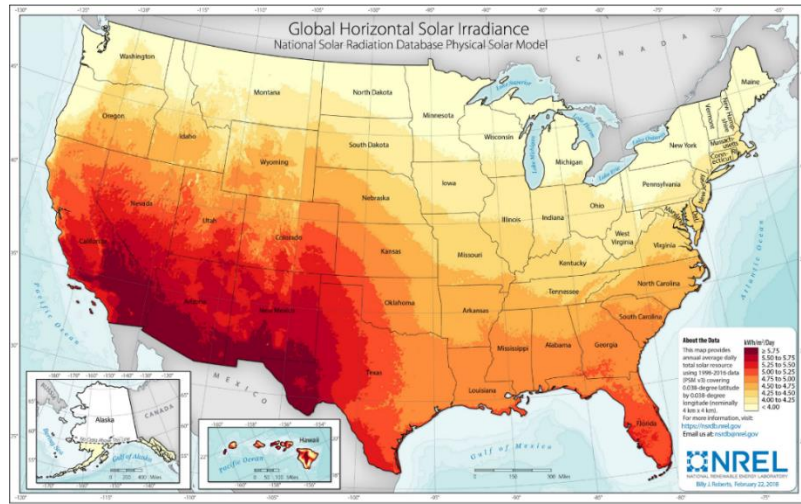


Figure 1.1. Contour map of solar resources in the United States However, effectively harnessing the United States' solar resources is not without significant challenges as solar irradiation is dilute, unequally distributed, and intermittent

However, harnessing this potential energy has challenges as solar energy is dilute, unequally distributed, and intermittent¹. Concentrating solar irradiation can be a possible solution to the unequally distributed and dilute solar power we see across the U.S. One technology that has been gaining traction is the use of Concentrated Solar Power Plants shown in Figure 1.2.



Figure 1.2: Noor Concentrated Solar Power Plant in Morocco

Concentrated solar power (CSP) makes use of large flat space and many heliostat reflectors to reflect light to a tower, where it can be stored or converted to electricity. In 2014, concentrated solar plants made up 8% of the world's renewable energy². In order for these technologies to be used widely, more innovation is needed in the plant components to reduce costs as well as increase the efficiency of the solar receivers.³ Other technologies that concentrate solar irradiation for various applications are shown in figure 1.3⁴.

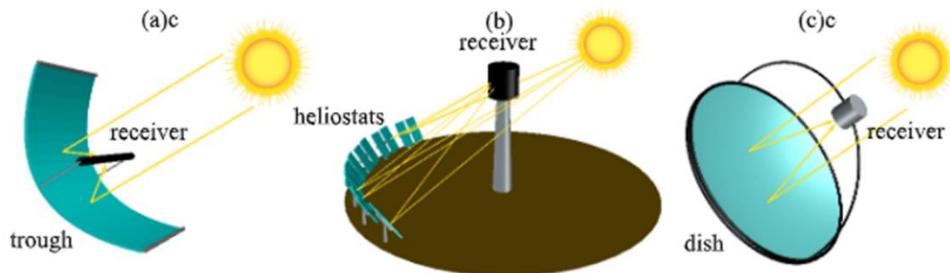


Figure 1.3: Schematics of the principal solar concentrating technologies: (a) parabolic trough system, (b) tower system, and (c) a paraboloidal dish system with the rays from the sun representing reflection paths from the mirrors.

Testing these technologies is necessary for them to be improved, but because of the dilute nature of solar irradiation these tests can be difficult. A solar simulator is a device that provides a light source that is like natural sunlight in both intensity and spectral distribution. Solar simulators offer affordable, consistent, and accurate simulation of the power tower and parabolic dish solar concentrators depicted in figure 1.3.

1.2 Objectives

The purpose of this study was to design, model, and test a High Flux solar simulator for various experiments needing testing under high intensity radiation with a spectral distribution similar to the sun. This simulator design features four 2.5kW metal halide lamps each with elliptical reflectors and placed on pedestals that will allow them to be manually adjusted in 3 degrees of motion. A fifth 3kW xenon arc-lamp will be added to the simulator featuring a parabolic reflector and secondary concentrator lens. This central lamp will be placed on a linear actuator to allow the user to move the lamp horizontally away from the focal point. Doing this will make it so the user can vary the power the central lamp provides to the system allowing for extra adjustability by alternating the flux shape. The simulator is modeled using Monte Carlo Ray Tracing (MCRT) to accurately create flux maps and estimate the power, peak flux, and area of the simulator. These thesis objectives are as follows:

1. Construct four 2.5kW metal halide lamp housings
2. Design and construct a 3kW xenon lamp placed on a linear actuator for horizontal translation in order to alter the flux map shapes

3. Keep the simulator affordable and reduce complexity by using off the shelf components whenever possible
4. Creation of a detailed MCRT simulation model that accurately represents the radiative exchange of the simulator
5. Design and construct the full simulator with user friendly maintenance capabilities and proper safety precautions

1.3 Thesis Overview

A combination of modeling and experimental work was performed to achieve the thesis objectives. Chapter 2 includes an extensive literature review: 1) state-of the art solar simulators for simulating concentrated solar power with an emphasis on simulators that have capabilities of varying flux, 2) A comprehensive comparison of metal halide and xenon lamps, 3) A comparison of primary and secondary reflectors.

In Chapter 3, the basic principles of MCRT are explained in detail. This explanation of MCRT is broken into four parts. The first is an explanation on random point generation on surfaces and emission from that surface. Second explains the method of tracing this ray to the next surface. Next, the absorption or reflection of the ray once it hits the surface. And finally, a definition of participating media and its impacts on the traveling ray.

In chapter 4, the designs of the individual lamp housings are shown in more detail. This will show some of the design decisions made and talk about some of the features that make these individual housings unique. This chapter will also feature the specifics of MCRT for these individual systems, going over how the arc was modeled, the reflection off of the specific reflectors, as well as the participating media that exists in

these systems. Results of the MCRT for the individual housings will also be presented here.

In Chapter 5, the design, alignment, modeling, and results of the modeling for the whole simulator are presented. The design will discuss how the five lamps in the simulator come together and the degrees of motion that exists for each. Alignment is the process of moving the lamps to their proper position, and the methods used to accomplish this. Modeling will take the individual models created in the previous chapter and bring them together with angular and linear transformations. Finally, the results of this model will be presented. Flux maps showing the peak flux, aperture size, and the total power within it will be presented at the focal point as well as various distances in front and behind it. The effect of the focal plane will also be analyzed depending on the location of the central xenon lamp.

In Chapter 6, the study conclusions and technical contributions to the field were reviewed. Recommendations for future work and research opportunities which have been produced from this work were presented.

CHAPTER II

LITERATURE REVIEW

2.1 Review of Other Simulators

Solar simulators consist of 5 major components. The light source, the reflector/concentrator, the Lambertian target, a calorimeter, and a CCD camera. As this field continues to grow many researchers and universities have begun to create their own solar simulators, but there has yet to be a common, inexpensive, and commercially available simulator. Table 2.1⁵ below shows other simulators and important aspects to note about them.

Table 2.1: A review of notable simulators and some of their important features. Notably the lamp type, the concentrator shape, the peak flux, and the spot.

Place	Year	Power	Radiative Power	Efficiency	N. of Lamps	Lamp Type	Concentrator Shape	Peak Flux	Spot(mm)
CIEMAT	N.A.	4	1.21	30.2%	1	4 kW xenon	Ellipsoid	1400	35x35
IMDEA	2009	7	2.1	30%	1	7 kW xenon	Ellipsoid	2700	N.A.
Texas A&M Qatar	2013	7	1.64	47%	1	7 kW xenon	Ellipsoid	3583	220
Niigata Univesity	2006	5	0.368	7.4% (18.3%)	1	5 kW (6 kw) xenon	Ellipsoid	784 (2300)	60 (40)
Berkeley Laboratory	1991	20	3	15%	1	20 kW xenon	Ellipsoid	16000	70 x 70
ETH	2003	200	75	37.5% (5.4%)	1	200 kW argon	Ellipsoid trough	>5000 (3250)	N.A. (60)
Niigata University	2012	18	3.2	17.8 (24.3)	3	6 kW (7kW) xenon	Ellipsoid	2085 (4225)	60 (90)
Niigata University	2013	133	33.3	25%	19	7 kW xenon	Ellipsoid	>3000	200
TIT	2003	10	2	20%	2	5 kW xenon	Ellipsoid	N.A.	8
DLR	2007	60	21	33.3%	10	6 kw Xenon	Ellipsoid	N.A.	100 cm ²
PSI	2007	150	50	33.3% (13.3%)	10	15 kW xenon	Ellipsoid	11000	240 (60)
Minnesota University	2010	45.5	9.2	20.2%	7	6.5 kW xenon	Ellipsoid	7300	60

Florida University	2010	42	N.A.	N.A.	7	6 kW xenon	Ellipsoid	N.A.	N.A.
IMDEA	2013	42	14	33.3% (12.6%)	7	6 kW xenon	Ellipsoid	3600	200 (60)
GIT	2015	42	6	14.3%	7	6 kW xenon	Ellipsoid	>6500	40
KIER	2015	N.A	16.9	N.A.	3	Xenon	Ellipsoid	3019	N.A.
ANU/EPFL	2015	45	10.6	23.6 (10.4)	18	2.5 kW xenon	Ellipsoid	9500	60 (30)
IET	2010	28	6.4	22.9%	4	7 kW xenon	Ellipsoid	N.A.	300
KTH	2013	84	19.7	23.4%	12	7 kW xenon	Paraboloid + Fresnel lens	6730	200
Zhejiang University	2013	35	5	14.3%	5(+1+1+1+1)	7 kW (+10+5+3+1) kW xenon	Ellipsoid (spherical reflectors)	700	100
Swinburne University	2014	42	12	28.6%	7	6 kW Metal halide	Ellipsoid	927	175
Adelaide University	2015	6	1.2	20% (50%)	1 (7)	6 kW Metal halide	Ellipsoid + conical	700 2800	60
Sandia	2015	7.2	0.44	6.2%	4	1.8 kW Metal Halide	Ellipsoid	1140	25.4
MIT	2010	10.5	5.1	48.6%	7	1.5 kW Metal Halide	Ellipsoid + Hexagonal-Conical	60	380
JFCC	2014	100	8 at 75% of P_n	10.7%	20	5 kW xenon	Ellipsoid + Fresnel lens	37.7 (>90)	4000x70d (2000x30d)

Most of the simulators above feature xenon lamps with ellipsoid reflectors and have little to no spot adjustability. There are simulators that have unique designs specifically to add this capability. A few are shown in figure 2.1.

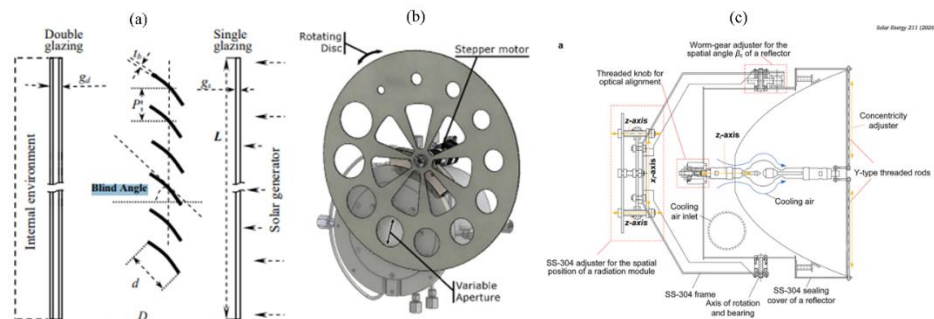


Figure 2.1: Simulators with flux aperture adjustments: a) Venetian blind, b) rotating disk, c) variable reflector

In the above figure on the left you can see a venetian blind which can be angled to control the amount of solar radiation making it through.⁶ In the middle, you can see a rotating disk design with the radius getting smaller as the disk rotates in front of the reactor.⁷ Finally, on the right, you can see a design that bends the reflector in order to change the reflector geometry and the way light is reflected off of it.⁸

2.2 Metal Halide Vs. Xenon Lamps

Table 2.1 shows that the most common lamps used for solar simulators are xenon and metal halide lamps which can be shown in figure 2.2²

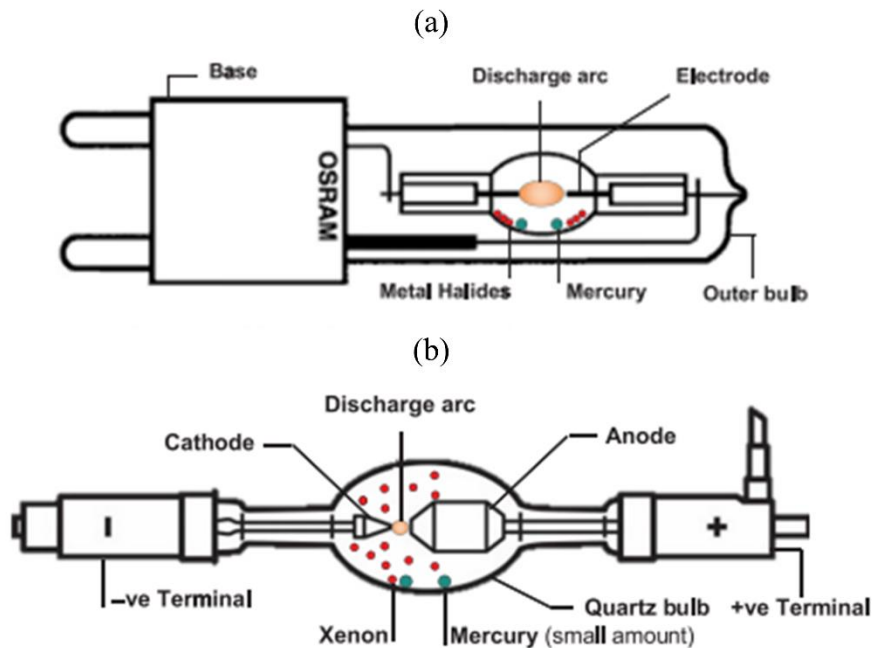


Figure 2.2: Metal-Halide (top) and xenon arc (bottom) lamps

Both lamps in the figure ignite the gas inside to create plasma. The geometry of the metal halide bulb makes it an easier to fit in a reflector because there is no need to

support it from the front. The xenon lamp has a smaller arc size and a spectral distribution that closely matches the sun as shown in Figure 2.3.⁹

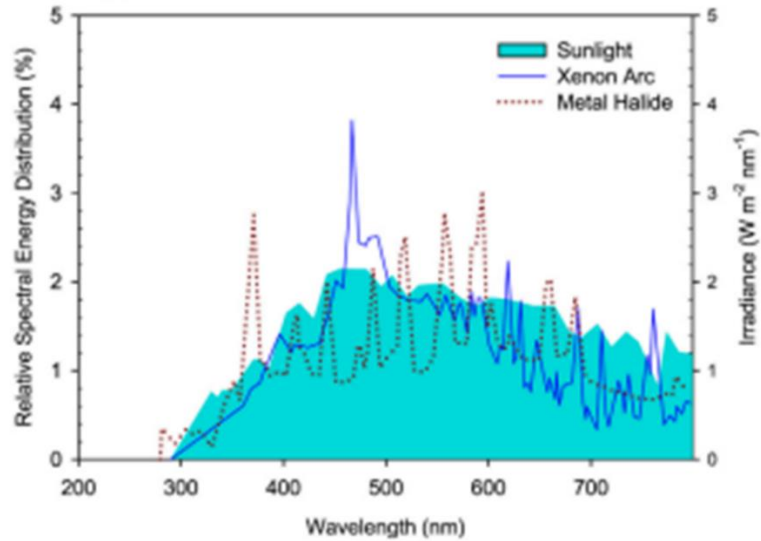


Figure 2.3: Spectral distribution of sunlight, xenon arc lamp, and metal halide lamp with Irradiance and relative spectral energy distribution on the Y axis and Wavelength on the x axis

The above figure shows the spectral distribution of sunlight and both lamps. While both offer good approximations of sunlight, the metal halide distribution lacks in the 400 – 550 nm range. This is where the irradiance of the sun is strongest so it is a particularly important area. The xenon spectrum is more consistent across the wavelengths with less large spikes like the metal halide. Although metal halide lamps have larger arcs, and less ideal spectral distributions they make up for it in their efficiency and costs. Table 2.2 shows a breakdown of these properties.

Table 2.2: Cost analysis of Xenon vs. Metal Halide Lamps

Lamps	Power	Efficiency	Efficient Power	Cost	Price per kW
-------	-------	------------	-----------------	------	--------------

Xenon	3kW	50%	1.5kW	946.65\$	473.3\$/kW
Metal Halide	2.5kW	80% ¹⁰	2kW	422.99\$	211.5\$/kW

Finally, varying the power supplied to the lamp will not vary the intensity of the radiation from the lamp. Metal-Halide lamps are a more cost-effective option when compared to Xenon-lamps. They also emit light in a spectrum that is very close to sunlight, although they experience gaps at certain wavelengths. They also have a long-life span and experience less change in color and loss of intensity as time goes on.² The use of Metal Halide lamps for HFSS applications has become more common in the last 12 years after MIT was able to make a seven-lamp solar simulator for less than 10,000\$.⁵

2.3 Primary and Secondary Concentrators

The next way designs often display variations from each other is the type of reflector being used. One type of reflector is an ellipsoidal reflector shown in figure 2.4.

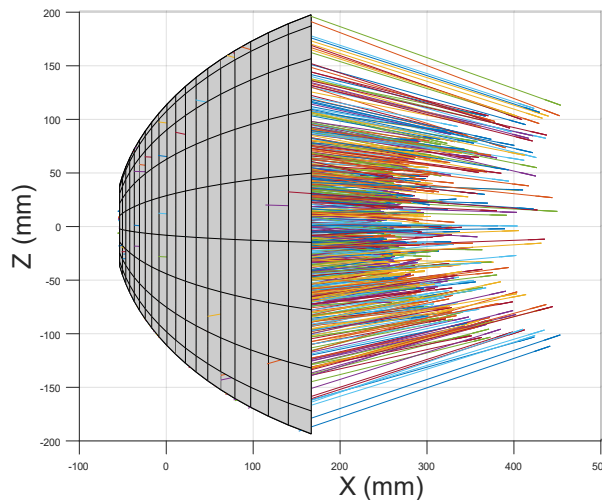


Figure 2.4: Elliptical Reflector

As shown in the figure ellipsoidal reflectors are angled in such a way that when a source of light is placed at the focal point inside of the reflector it will reflect off the reflector in such a way that it then hits the other focal point. In the figure above the source focal point is at 0mm which then reflects and join at the second focal point roughly 800mm away. Figure 5 shows a parabolic reflector with the addition of a secondary concentrator lens.

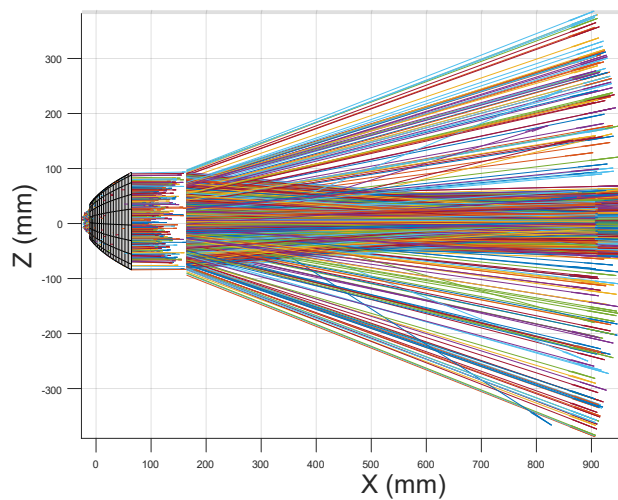


Figure 2.5: Parabolic reflector with secondary concentrator lens

As you can see from the figure parabolic reflectors are angled in such a way that the light reflects off in parallel lines. Then with the use of the secondary concentrating lens, the radiation can be focused to a point, in this case it is roughly 800mm in front of the lens. Both reflectors make use of a silver or aluminum coating to create the reflective surface required.

CHAPTER III

MONTE CARLO RAY TRACING

To help aid with the design and characterization of the simulator a Monte Carlo Ray Tracing algorithm was created to give an idea of what kind of flux maps the simulator will generate in an ideal scenario. MCRT makes use of physics-based radiative exchange equations changed to cumulative distribution functions that can use random uniform distributions to predict the properties and behaviors of an individual ray. A ray is defined by the following equation.

$$r = x, y, m, n, o \quad (3.1)$$

Where x,y,z describes the origin/location in space and m,n,o describes the rays direction. A depiction of this ray can be shown in the figure 3.1 below

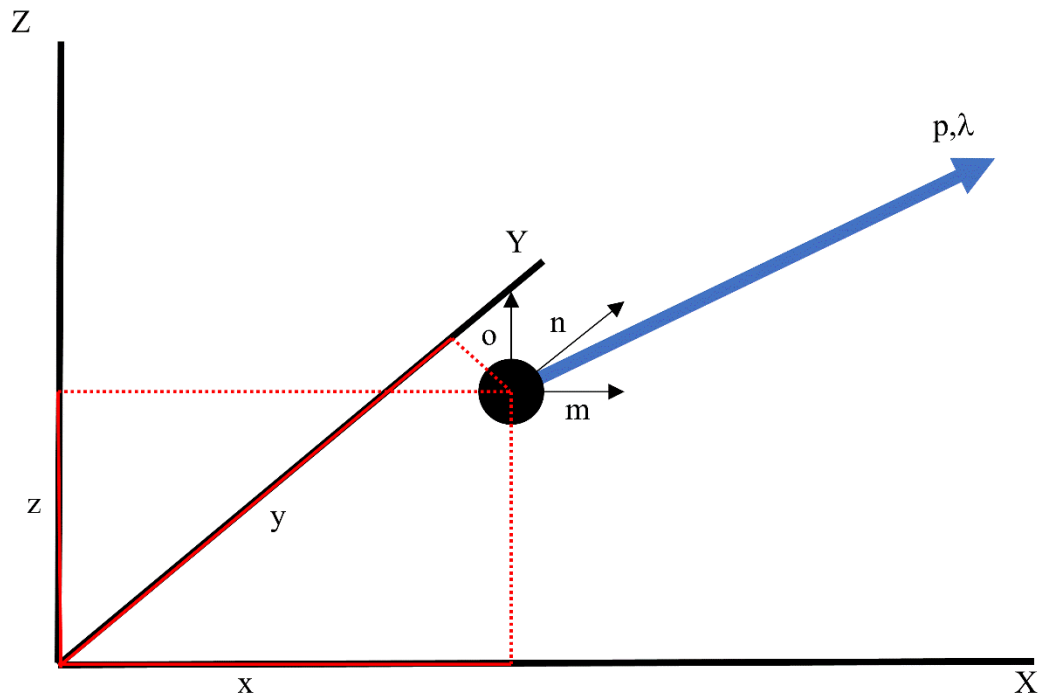


Figure 3.1: visualization of a single ray leaving a point. It is defined by its position x,y,z and its direction m,n,o it also is assigned a wavelength and carries a set amount of power

Two categories of ray tracing, surface ray tracing where you are looking at the radiative exchange between surfaces, and there is participating media where the space between surfaces is composed of absorbing and scattering media. Surfaces are defined with the use of surface functions.

$$S(x, y, z) = 0 \quad (3.2)$$

Participating media refers to materials that absorb, emit, and scatter radiation within the volume they take up. They also refract and reflect radiation when it first contacts the media. The process of emitting and tracing rays can be done millions of times in order to accurately capture the radiative exchange process.

3.1 Surface Emission

When a ray is emitted from a surface there are 3 different random properties that need to be chosen. Position, direction, and wavelength. Positions need to be generated to accurately represent a uniform distribution of points over a surface area.¹¹

$$R_i = \frac{\int_0^i dA}{\int_0^l dA} \quad (3.3)$$

Once the random point is found the ray must be emitted in a random direction. First is to find a local coordinate system from the point of emission. This is done with a normal vector and two tangential vectors defined by the equations below.

$$n = \frac{\nabla s}{\|\nabla s\|} \quad (3.4)$$

$$t_1 = \frac{n \times axis}{\|n \times axis\|} \quad (3.5)$$

$$t_2 = t_1 \times n \quad (3.6)$$

Where n is the normal vector obtained by using the gradient of the surface s . t_1 is a tangent vector obtained by doing the cross product of the normal vector and $axis$ which is created by finding another point on the tangent plane. Finally, t_2 , the final tangent vector to create the coordinate system, can be created by doing the cross product of t_1 and n . Now that the reference plane has been defined the direction can be chosen with the following equations.

$$E_\lambda = \frac{E_{b\lambda}}{\pi} \int_0^{2\pi} \int_0^{\pi/2} \varepsilon_{\lambda,\theta} \cos \theta \sin \theta d\theta d\phi \quad (3.7)$$

Where E_λ is the point's emission as a function of wavelength, $E_{b\lambda}$ is the black body emission, $\varepsilon_{\lambda,\theta}$ is the surfaces emissivity as a function of wavelength and angle θ . θ is the polar angle and ϕ is the azimuth angle. Shown in figure 3.2 below

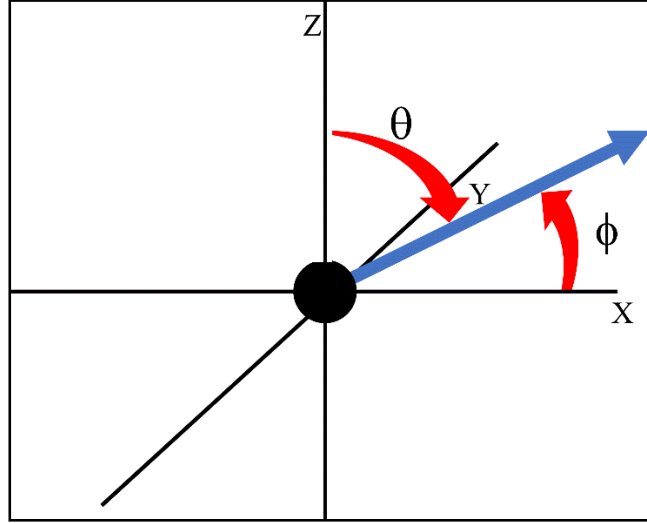


Figure 3.2: Visualization of angles ϕ and θ

The angle ϕ represents the angle in the x,y plane and is between 0 and 2π . The angle θ is in the z,x comes out from the surface between 0 and $\pi/2$. These two angles can be found with the equations below.

$$\phi = 2\pi R_\phi \quad (3.8)$$

$$\theta = \sin^{-1}(\sqrt{R_\theta}) \quad (3.9)$$

Where R_ϕ and R_θ are random numbers between 0 and 1. These numbers can be used to diffusely emit from a coordinate plane. The last part of emission is choosing a random wavelength for the ray to emit at. This can be done with the equations below.

$$R_\lambda = \frac{1}{\epsilon T^4} \int_0^\lambda \epsilon_\lambda E_{b\lambda} d\lambda \quad (3.10)$$

After inversion,

$$\lambda = \lambda(R_\lambda, x, y) \quad (3.11)$$

Since we will only be looking at isothermal surfaces with constant emissions the equation can be simplified

$$R_\lambda = \frac{1}{\sigma T^4} \int_0^\lambda E_{b\lambda} d\lambda = f(\lambda T) \quad (3.12)$$

3.2 Tracing

After the ray has been emitted the next step of the MCRT process is to follow the ray to the next surface. A ray has reached a surface when the surface equation is 0 shown in equation 3.2. When solving for when the ray will hit a surface you will get a value τ which represents the amount of distance the ray had to travel before coming into contact with the surface. To get τ the following substitution can be performed.

$$x = x_0 + \tau u \quad (3.13)$$

$$y = y_0 + \tau v \quad (3.14)$$

$$z = z_0 + \tau w \quad (3.15)$$

Where $x_0, y_0,$ and z_0 is the location the ray starts from, and $u, v,$ and w is the rays direction. By subbing these equations in for $x, y,$ and z in the surface equation you will get an equation that can be solved for τ . A τ value will be calculated for every surface making sure to ignore imaginary and negative numbers because although negative τ can be calculated in reality a ray cannot travel backwards. Once all the τ 's have been calculated the smallest value will tell you which surface is contacted first.

3.3 Absorption, Reflection

Once the ray has been traced to its surface the ray can either be reflected or absorbed. To determine this the absorbance (α) of the surface must be known. With this the following check can be done to determine the outcome.

$$R \leq \alpha \rightarrow \text{bundle absorbed} \quad (3.16)$$

$$R > \alpha \rightarrow \text{bundle reflected} \quad (3.17)$$

Where R is a random number between 0 and 1. Now if the ray is reflected there are two different ways the reflection can occur, diffuse reflection and specular reflection. Diffuse reflection is done the exact same way emission is done and can use equations 3.7, 3.8, and 3.9. If the reflection is specular the following equation can be used to determine the new path.

$$\hat{r} = u - 2(u \cdot n)n \quad (3.18)$$

Where n is the normal vector from the reflective surface, u is the vector of the ray before reflection, and \hat{r} is the direction of the vector after reflection.

3.4 Ray tracing through Participating media

As the ray travels in space may encounter a number of different materials. Some of these materials are classified as participating media and act differently. When first interacting with one of these surfaces the ray may experience a change in direction due to Snell's law shown below in the equation¹²

$$n'(s' \times g) = n(s \times g) \quad (3.19)$$

Where n' is the refractive index of the surface being entered, s' is the vector after the ray has been refracted, g is the normal vector at the position of refraction, n is the

refractive index of the material the ray is leaving and s is the initial vector of the ray. A helpful visual of this is shown in figure 3.3¹³ below

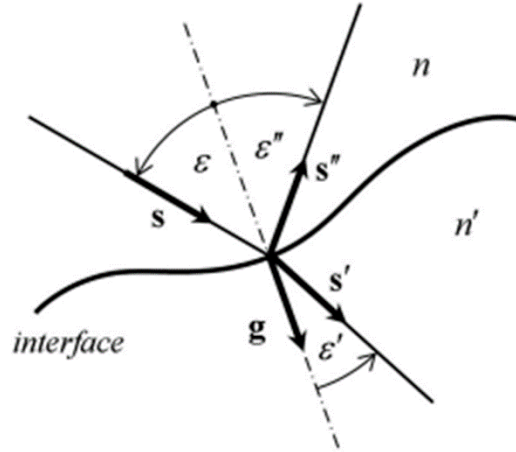


Figure 3.3 Reflection and refraction at the interface between two optical media with different refractive indices.

Also shown in the figure it is possible for the ray to reflect, in which case, it will experience specular reflection. The properties reflectance of the material can increase depending on the angle the ray approaches at.

$$\rho_{\parallel} = \left(\frac{\cos \epsilon' - n \cos \epsilon}{\cos \epsilon' + n \cos \epsilon} \right)^2 \quad (3.20)$$

$$\rho_{\perp} = \left(\frac{\cos \epsilon - n \cos \epsilon'}{\cos \epsilon + n \cos \epsilon'} \right)^2 \quad (3.21)$$

$$\rho = \frac{1}{2} (\rho_{\parallel} + \rho_{\perp}) \quad (3.22)$$

Where n is the refractive index of the material, and ϵ and ϵ' are the corresponding angles shown in figure 3.3. While the ray is inside the participating media the

absorptance of the material increases as a function of the distance traveled through it.

This can be quantified in the equation below.

$$a_{\Delta\lambda}(s_a) = 1 - e^{-k_{\Delta\lambda}s_a} \quad (3.23)$$

Where $a_{\Delta\lambda}$ is the absorptance as a function of distance, k is the absorptance of the material, and s_a is the distance traveled inside of it. Solving the equation for s_a and equating $a_{\Delta\lambda}$ to a random number of yields

$$s_a = -\frac{1}{k_{\Delta\lambda}} \ln(1 - R_a) \quad (3.24)$$

CHAPTER IV

INDIVIDUAL LAMP HOUSINGS

4.1 Design of Metal Halide Housing

The simulator presented features four 2.5 kW metal halide lamps shown in figure 4.1.

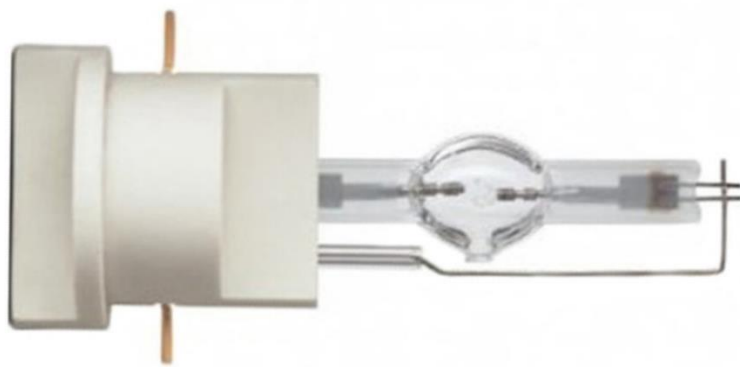


Figure 4.1: Philips MSR Gold 2.5kW FastFit metal halide lamp

This lamp comes with a lamp socket that is designed so the lamp can easily be installed. The reflector used is an elliptical reflector from optiforms shown in figure 4.2

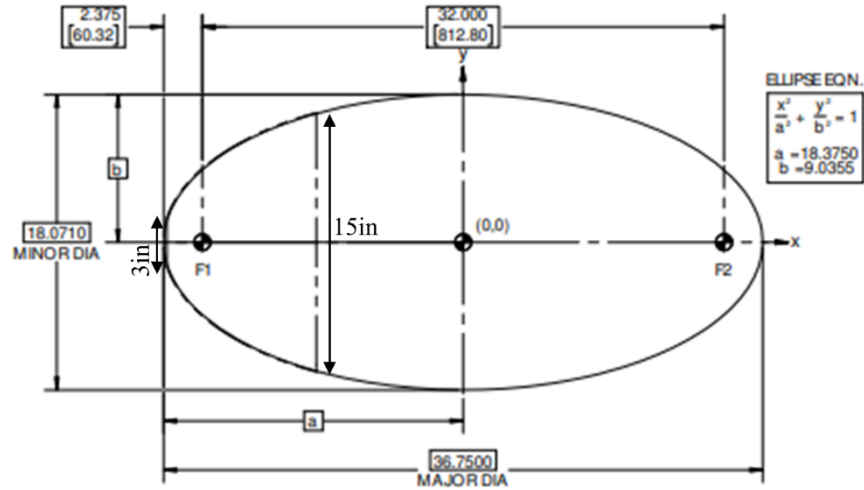


Figure 4.2: Optiforms E813 reflector with a 32 inch focal length a front diameter of 15 inches and a back diameter of 3 inches

This reflector has a 32-inch focal point distance, 15-inch front diameter and 3-inch back diameter. It has a high reflective silver coating. The reflectance of which is shown in figure 4.3 below.

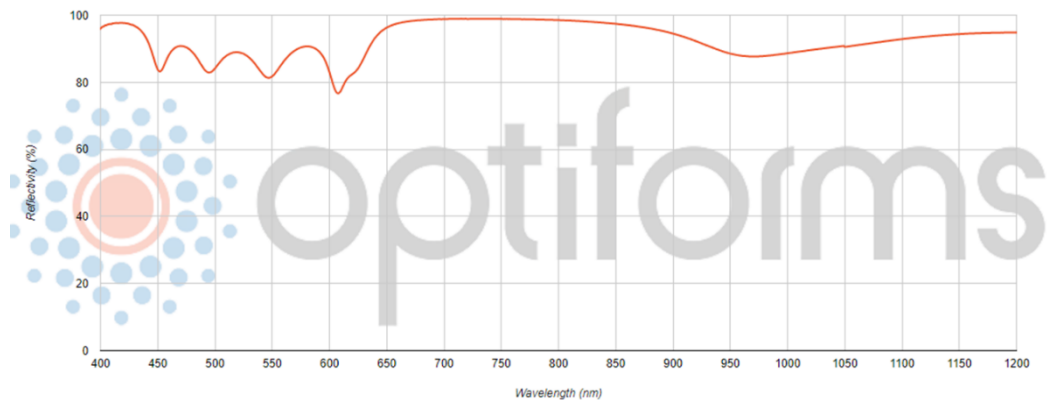


Figure 4.3: Reflectivity vs. wavelength of optiforms reflective silver coating

The reflectance of this coating remains above 80% for the fast majority of wavelengths that the lamp will emit. A view factor calculation was done to determine

how well the rays will hit this reflector. This view factor calculation was found from the University of Texas Austin database of view factors, specifically, the coaxial disk to coaxial disk and was calculated to be around 75%. Figure 4.4 shows the SolidWorks rendering of the metal halide lamp housing.

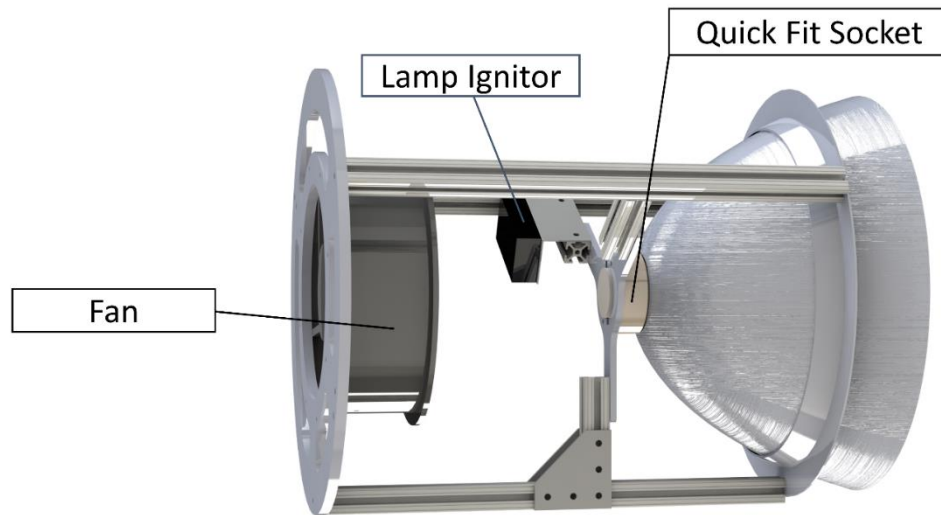


Figure 4.4: Metal Halide lamp housing

This figure does not show the metal sheath that is wrapped around the housing to enclose it for safety and promote air flow. The fan is placed at the base of the housing and provides airflow to the ignitor and the back of the reflector. The lamp socket has the ability to be pulled back away from the reflector in the event you need to see inside or if small adjustments need to be made. The reflector is held in place by a reflector ring designed and accurately installed by Opti forms. To get the quick fit socket in place a measurement from the base of the housing was made to move the aluminum extrusion forward.

4.2 Monte Carlo of Metal Halide Housing

This section will go into more detail about the specifics of modeling the metal halide lamp module. Specifically, the arc model used for source generation of the metal halide lamp and the way the rays reflect off the ellipsoid reflectors. This arc model was made of a series of 9 nested ellipses¹⁴ shown below in figure 4.5

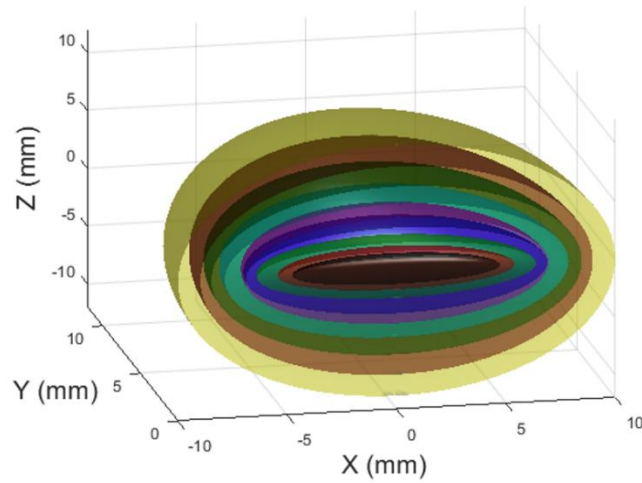


Figure 4.5: Arc model of metal halide lamp, it is a series of 9 nested ellipses

This arc model shape has shown to increase accuracy of MCRT for metal halide lamps. To generate random points on an ellipse the following equations were used.

$$x = a\xi \cos \phi \quad \phi = 2\pi R \quad \xi = \sqrt{R} \quad (4.1)$$

$$y = rad \sin \theta \quad rad = \sqrt{b^2 - \frac{b^2}{a^2} x^2} \quad \theta = 2\pi R \quad (4.2)$$

$$z = rad \cos \theta \quad rad = \sqrt{c^2 - \frac{c^2}{a^2} x^2} \quad \theta = 2\pi R \quad (4.3)$$

Where ϕ is the azimuth angle, θ is the polar angle, a, b , and c are the dimensions of the ellipse, R is a random number between 0 and 1. Each R in the above equations are generated individually. Next, the ray is traced to either the ellipsoidal reflector or to the planes cutting the front and back of the reflector. The surface equation for the ellipsoidal reflector is shown below in Equation 4.4.

$$S_{ellipse} = \frac{x^2}{a^2} + \frac{y^2}{b^2} + \frac{z^2}{c^2} - 1 = 0 \quad (4.4)$$

Once x , y , and z have been substituted by the equation shown in 3.12, 3.13, and 3.14 the following equation can be derived.

$$S_{ellipse\tau} = \left(\frac{u^2}{a^2} + \frac{v^2}{b^2} + \frac{w^2}{c^2} \right) \tau^2 + \left(\frac{2ux_0}{a^2} + \frac{2vy_0}{b^2} + \frac{2wz_0}{c^2} \right) \tau + \frac{x_0^2}{a^2} + \frac{y_0^2}{b^2} + \frac{z_0^2}{c^2} - 1 = 0 \quad (4.5)$$

This equation can be solved for τ using the quadratic formula. The other surface rays can come in contact with are planes with surface equation shown in equation 4.6.

$$S_{plane} = A(x - x_c) + B(y - y_c) + C(z - z_c) = 0 \quad (4.6)$$

Where A,B and C are the intersection points of the plane on the X,Y and Z axis. For the planes used in this MCRT A=1, B=0, and C=0. This simplifies the plane's surface equation to equation 4.7

$$S_{plane} = x - x_c = 0 \quad (4.7)$$

Once x has been substituted with equation 3.12 the following equation is derived.

$$S_{plane\tau} = x_c - x_0 - \tau u = 0 \quad (4.8)$$

Once the ray has been traced if it hits the reflector it can experience reflection or absorption. A random number is assigned to the ray, if this number is higher than the reflectance of the reflector at that wavelength then the ray is absorbed. If not, the ray is reflected and experiences specular reflection. Figure 4.6 below is a visual of specular reflection.

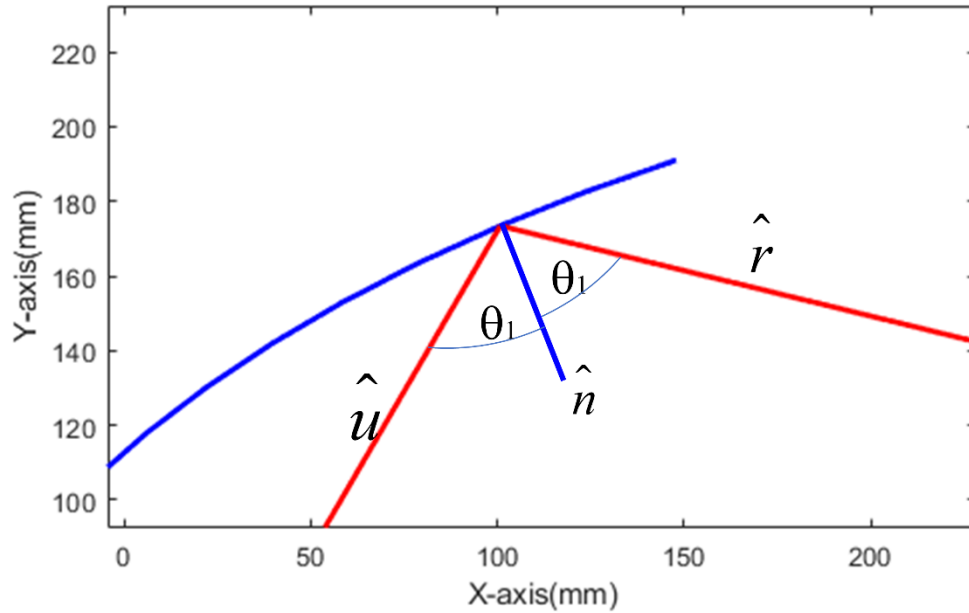


Figure 4.6: Specular reflection off an ellipsoidal reflector; u is the incoming ray r is the reflected ray and n is normal vector

The equation to perform this specular reflection is shown below in equation 4.9.

$$\hat{r} = u - 2(u \cdot n)n \quad (4.9)$$

Where \hat{r} is the vector of the reflected ray, u is the vector of the emitted ray, and n is the normal vector of the reflector. Once this is done results can be moved to a text file to be traced and sorted at the Lambertian target.

4.3 Design of Xenon Lamp Housing

The lamp used for this housing is a Philips LTI 3kW-HS Standard Xenon Lamp shown in figure 4.7 below.



Figure 4.7: Philips LTI 3kW-HS Standard Xenon Lamp with the cathode end on right and anode end on left

After starting with this xenon lamp the next step was to choose a reflector. The same view factor calculations done before were done with all of the reflectors optiforms has available and placed in a table. Table 4.1 shows some of the reflectors, their back diameters, focal length, view factor.

Table 4.1: Reflectors and view factors

	Back Diameter	Focal Length	View Factor
P19	0.875	0.75	0.842921479
P19-03	1.75	0.75	0.736427715
p23	1.3	0.9	0.808598492
p23-01	2.75	0.9	0.632421432
p23-02	2.25	0.9	0.686767231
P23-03	2.25	0.9	0.715606401
P25	0.5	1	0.842247627
P25-01	0.5	1	0.842247627
p25-02	2	1	0.71076473
p25-04	1.417	1	0.765156542
p33-01	2.5	1.3	0.684388118
p33-02	3	1.3	0.609536712
p33-03	1.75	1.3	0.684257816
p33-04	2	1.3	0.659300984
p33-05	1.625	1.3	0.673704804

Unfortunately, the reflectors with the best view factors in this table were also the reflectors with the smallest back diameters. Because of this the reflectors with the best view factors were not able to fit the xenon lamps inside of them. Models of each of the reflectors were created in solid works and the desired xenon lamp was fit inside to see if it would be able to fit. This finally narrowed down the reflector to a select few. The final criteria needed to be met was that the reflector used needed to have an equal or smaller diameter to the lens chosen. The lens chosen was a 200mm convex lens from Edmund optics with an 800mm focal length. It was rather difficult finding a large lens that was also affordable. This narrowed the reflectors down in the table to the P23-01 reflector which had a view factor of 60.32%. In the future, the hope is to be able to find a larger lens and choose a more desired reflector.

The next step when designing the xenon housing was to find a proper way to hold the lamp in place. After consulting prior literature, it is shown that most simulators featuring a xenon lamp are supported on the cathode end with a yoke, and on the anode end with a threaded insulated connection. One goal of this project was to maximize the amount of off the shelf components purchased for quality and repurchase ability. Because of these criteria added we looked for a company that sold these components commercially. This search led us to Strong Lighting, a projector company who was able to sell us their components used in their Gladiator 3 cinema projector. With these components we were able to assemble the “bulb support assembly” shown in Figure 4.8 below.

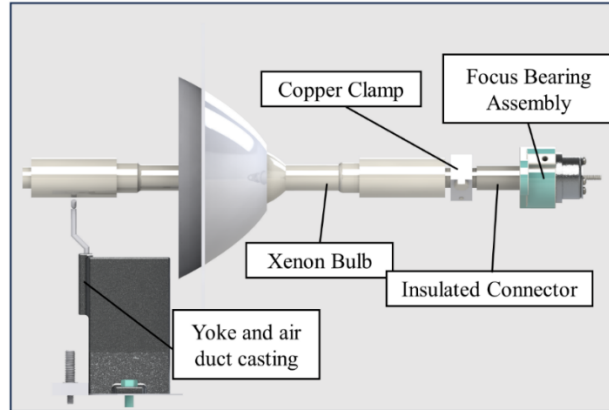


Figure 4.8: Xenon lamp support assembly from strong lighting with focus bearing assembly for small lamp adjustments

This bulb assembly has many features, the main being the ability to offer small lamp adjustments. A copper block clamps around the end of the lamp connecting it to an insulated tube to prevent conduction. The full housing for the xenon lamp is presented in figure 4.9 below.



Figure 4.9: Xenon housing placed on pedestal with linear actuator for horizontal translation

The housing for the xenon lamp is shown above. The lamp is held by the aforementioned bulb assembly and the yoke bearing assembly. There are two blowers at the top of the housing for cooling and the ignitor is bolted to the wall near it. On the left of the housing is the lens which is bolted between two aluminum plates with cutouts to keep it from breaking. The whole design is placed on the linear actuator to provide horizontal translation for varying the flux.

4.4 Monte Carlo Ray Tracing of Xenon Housing

The MCRT of the xenon lamp features a different arc model than the other lamp represented above and features a concentrating lens that will act as a participating medium. In figure 4.10 the model for a xenon arc-lamps source is shown.

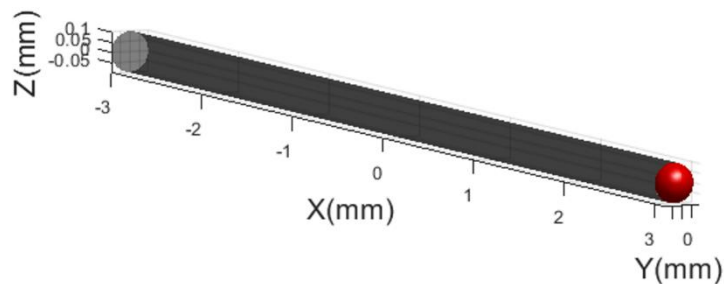


Figure 4.10: Xenon arc model consisting of a cylinder and sphere at the end

This model consists of a cylinder with a radius of 0.1mm and a length of 6mm. It also features a sphere of the same radius placed at the anode end of the source. Adding this sphere better represents the geometry of the arc because it captures the way radiation leaves the sharper point of the anode end of the lamp. The ray starts with the same process as the metal halide module in 4.2 with generation and emission. To generate random points on a cylinder the equations below are used

$$x = \left(x_0 - \frac{h_0}{2} \right) + R_h \quad R_h = Rh_0 \quad (4.10)$$

$$y = y_0 + r_0 \cos \phi \quad \phi = 2\pi R \quad (4.11)$$

$$z = z_0 + r_0 \sin \phi \quad \phi = 2\pi R \quad (4.12)$$

Where h_0 and r_0 is the height and radius of the cylinder. x_0 , y_0 and z_0 are the cylinders position ϕ is the angle at which the point lies on the circle, and R is the random number generated between 0 and 1. To generate random points on a sphere the following equations are used

$$x = r_0 \sin \theta \cos \phi + x_0 \quad \phi = 2\pi R \quad \theta = \pi R \quad (4.13)$$

$$y = r_0 \sin \theta \sin \phi + y_0 \quad \phi = 2\pi R \quad \theta = \pi R \quad (4.14)$$

$$z = r_0 \sin \theta + z_0 \quad \theta = \pi R \quad (4.15)$$

Once the cylinder and sphere have been generated the next steps are identical to the metal halide MCRT. The ray is traced, if it hits the reflector it checks to see if it is reflected or absorbed, if reflected its reflection is specular. A diagram of the system is shown in figure 4.11 below.

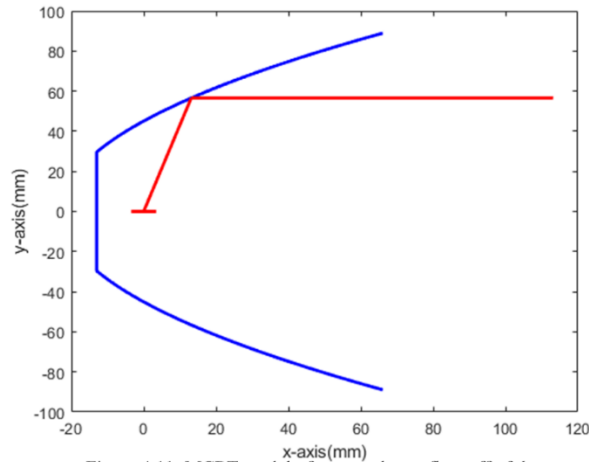


Figure 4.11: MCRT model of rays as they reflect off of the ellipsoidal reflector and make way towards the concentrating lens

The specular reflection off the parabolic reflector creates collimated beams of light that are then traced to the lens. The lens is made up of a cylinder, with a spherical surface on the reflector side, and a plane on the target side. The surface equation for the cylinder as a function of τ is

$$a = \left((d_{y1}w - d_{z1}v)^2 + (d_{z1}u - d_{x1}w)^2 + (d_{x1}v - d_{y1}u)^2 \right) \quad (4.16)$$

$$b = 2(d_{y1}w - d_{z1}v)(y_a z_b - y_b z_a - d_{z1}y_0 + d_{y1}z_0) + 2(d_{z1}u - d_{x1}w)(z_a x_b - z_b x_a - d_{x1}z_0 + d_{z1}x_0) + 2(d_{x1}v - d_{y1}u)(x_a y_b - x_b y_a - d_{y1}x_0 + d_{x1}y_0) \quad (4.17)$$

$$c = (y_a z_b - y_b z_a - d_{z1}y_0 + d_{y1}z_0)^2 + (z_a x_b - z_b x_a - d_{x1}z_0 + d_{z1}x_0)^2 + (x_a y_b - x_b y_a - d_{y1}x_0 + d_{x1}y_0)^2 - r^2 (d_{x1}^2 + d_{y1}^2 + d_{z1}^2) \quad (4.18)$$

$$S_{cylinder\tau} = a\tau^2 + b\tau + c \quad (4.19)$$

Where d_{x1} , d_{y1} , and d_{z1} is the distance the center axis of the cylinder travels on the x,y, and z axis. In this case d_{x1} is 2000 while d_{y1} , and d_{z1} are 0. x_a , y_a and z_a is the point at the beginning of the center axis and x_b , y_b and z_b are the points at the end of the center axis. Finally, x_0 , y_0 , and z_0 are the position of the cylinder in space and r_1 is its radius. The next set of equations is the surface equation for the sphere

$$a = u^2 + v^2 + w^2 \quad (4.20)$$

$$b = 2u(x_0 - x_c) + 2v(y_0 - y_c) + 2w(z_0 - z_c) \quad (4.21)$$

$$c = (x_0 - x_c)^2 + (y_0 - y_c)^2 + (z_0 - z_c)^2 - r^2 \quad (4.22)$$

$$S_{sphere\tau} = a\tau^2 + b\tau + c \quad (4.23)$$

The surface equation for the plane is the same as one in equation 4.8. Once the ray hits the lens directional reflection can occur the equations of which are shown in 3.20, 3.21, and 3.22. If the ray is transmitted through it experiences Snell's law shown in

equation 3.19. The ray is traced through the lens until it makes it to the other side where it either experiences directional reflectance and stays in the lens or transmits through and experiences Snell's law again on the way out. The whole time τ is being checked against the distance calculated from equation 3.24 if the number is smaller than the distance calculated the ray makes it through. Otherwise it gets absorbed somewhere inside of the lens.

4.5 Lamp Module Modeling Results

In this section, the flux maps produced from the MCRT of the individual lamp modules will be shown. Figure 4.12 shows the flux map of the metal halide lamp module.

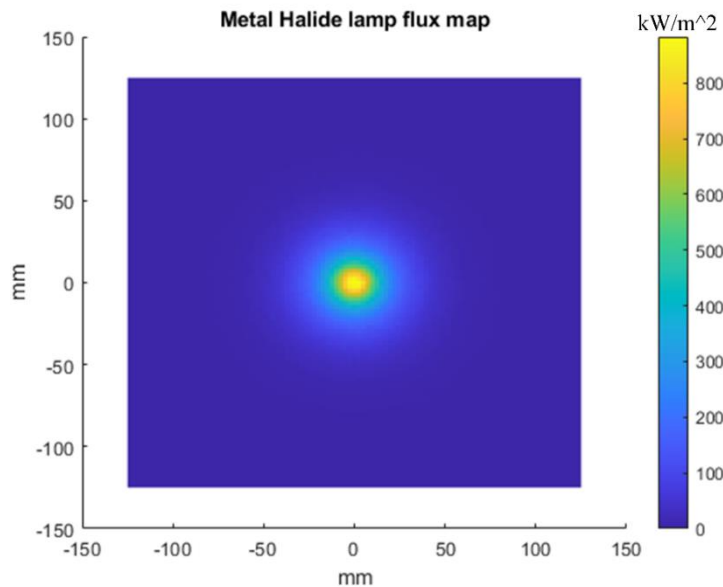


Figure 4.12: Flux map of metal halide module generated with MCRT; color bar on the left shows Flux in kW/m²; This shows a peak flux of 883kW/m² and a power of 0.8579kW in a 60mm aperture

As you can see the peak flux reaches 4000 suns and is in a 60mm aperture. The xenon lamp flux map is shown in Figure 4.13 below.

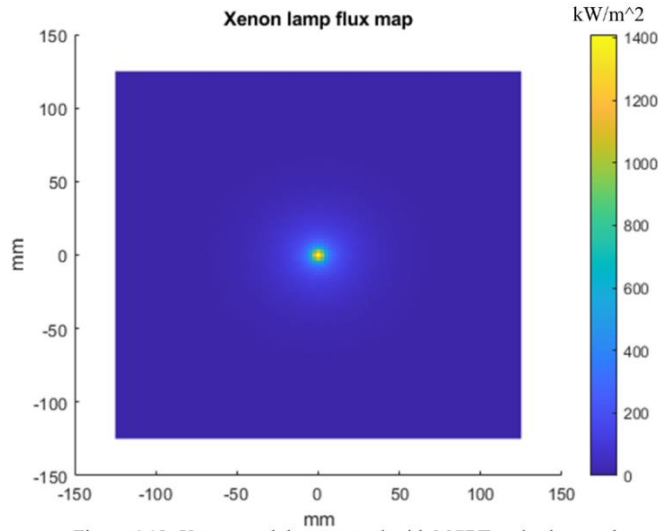


Figure 4.13: Xenon module generated with MCRT; color bar on the left shows Flux in kW/m²; The peak flux is 1409kW/m² and the power is 0.44kW in a 60mm aperture

As you can see from the flux map it has a peak flux of around 1400 suns and a much larger aperture size due to the concentrating lens. To determine if enough rays were used in this study the following figure 4.14 was made.

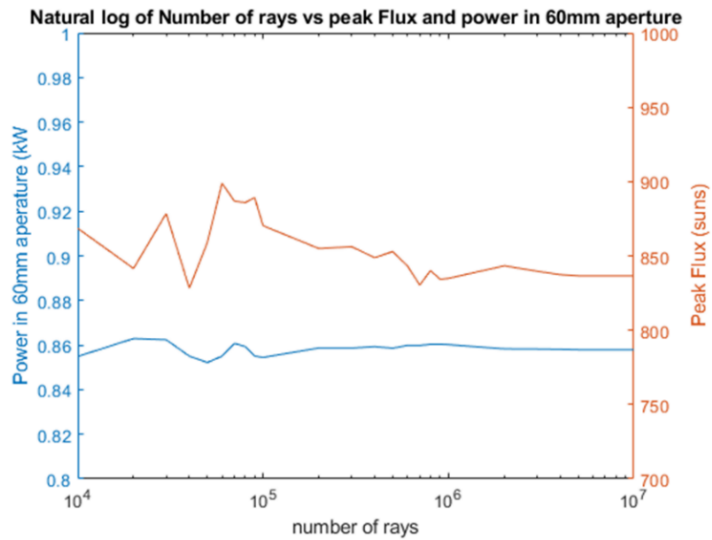


Figure 4.14: Plot of the number of rays vs peak flux and power in focal point; Number of rays is in a log scale and goes from 10 thousand to 10 million

5 million rays are enough to rays to accurately simulate the radiative exchange of these systems. The values no longer show noticeable differences after this point when increasing the number of rays simulated. This is what was used for this study. The next two plots in figure 4.15 show the effect of moving the xenon lamp on the flux map.

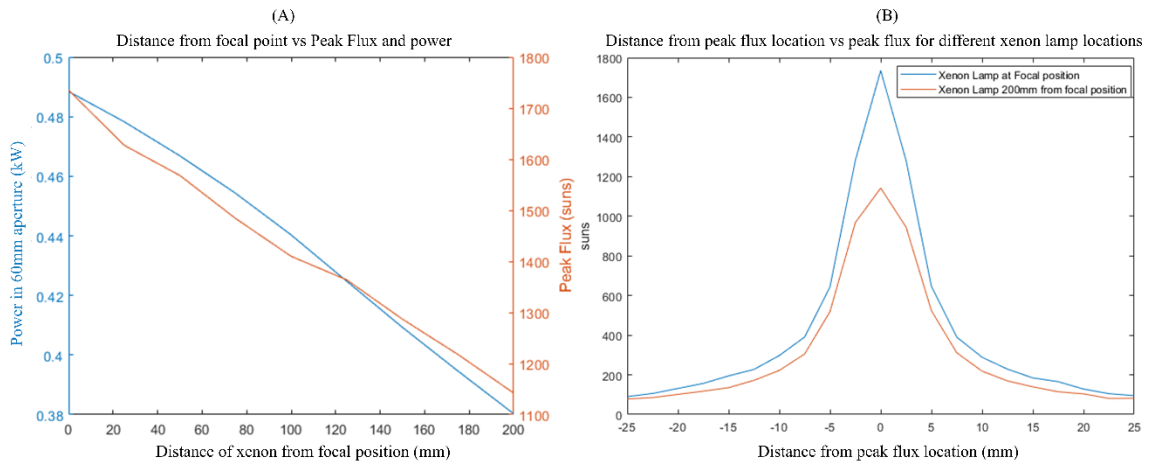


Figure 4.15: Plots showing effect of translating the xenon module; (A) Shows Distance of xenon from focal position vs Peak Flux and power; (B) Shows Distance from peak flux location on the target for the Xenon module at focal position and 200mm behind focal position

Plot A on the left shows the power and peak flux as a function of distance the xenon lamp has moved from the focal point. This plot shows the power in the aperture decreases about 0.11kW and peak flux decreases around 600kW/mm². Plot B shows the Flux as a function of distance from the peak flux location. The blue curve shows this with the xenon module at the focal position and the orange curve shows the module 200mm behind the focal position. This difference wasn't has exaggerated as expected, but power can still show that power and flux can be varied.

CHAPTER VI

FULL SIMULATOR

5.1 Design of Full Simulator

Figure 5.1 shows the design of the whole simulator.



Figure 5.1: Rendering of the 13kW high flux solar simulator

The whole simulator is placed in protective housing to keep people outside while it is running. The metal halide lamps are placed on rotating and translating platforms to be able to place them in the correct place. The pedestals can also be pulled back to allow the operator to work on one lamp individually. Shown in Figure 5.2



Figure 5.2: Side profile render of simulator with lamps pulled back

Being able to pull the lamps back allows for the simulator operator to easily focus on a housing individual without having to work around the other ones. With the addition of the xenon lamp, not shown in the figure above, the east and west lamps cannot be moved individually but only as a pair. Another aspect of adjustability in this simulator is the adjustable platforms of the metal halide lamps shown in figure 5.3.



Figure 5.3: Adjustable platform and linear stage for metal halide housing allowing for 3 degrees of motion.

This is the configuration of this platform for the north and south lamp, the adjustable platform in this case allows for the Lamp to be turned as well as tilted up and down. The east and west lamp have this lamp rotated 90 degrees This means the platform can move the lamps left and right, and rather than tilting up and down the lamp can be tilted left and right. The simulator was aligned starting with the top lamp. First using the linear stage, the lamp was brought as far forward as possible. Afterwards, using a digital angle level the housing was tilted down 27.8° . Next was to make sure the lamp was perpendicular to the irradiation zone. Using a automatic laser level a horizontal lamp was placed across the aligned across the back of the housing shown in figure 5.4.



Figure 5.4: Laser alignment procedure for top lamp. When the housing is positioned properly the laser will be able to cross both bolts on the back plate.

The horizontal laser level projects a horizontal laser. When the housing is perpendicular to the irradiation zone the laser will cross both bolts on the back plate. If the lamp is turned to the left or right the laser will not cross over both bolts. Once the top lamp was in position, 3 laser pointer mounts were placed on the aluminum extrusion of the housing to angle at the focal point of the reflector. A figure of the housing with the lasers on them is shown in Figure 5.5 below.

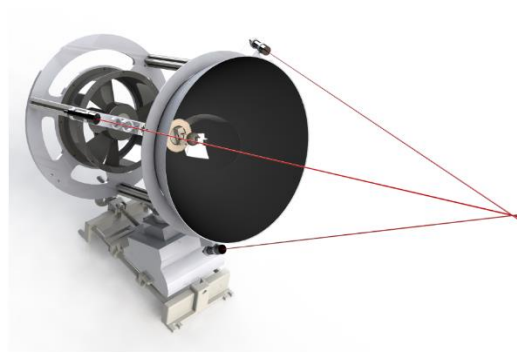


Figure 5.5: Laser point holders of single lamp angled to point at reflectors focal point.

The focal point was then marked on a plate. After, the laser pointers were moved to the other lamps which were adjusted until the lasers hit the same place. Figure 5.6 shows the full simulator with laser pointers attached.



Figure 5.6: laser pointers placed on all 4 metal halide housing for alignment

With the use of the laser pointers the simulator was aligned to the proper positions like the figure above.

5.2 Monte Carlo Ray Tracing of Full Simulator

To be able to extend the MCRT for the individual lamps to the full simulator output some translations were done to move the lamps into the right place. The north and the south lamp are both rotated around the Y axis and therefore have the same equations with opposite angles of rotation. Similarly, the east and west lamp are both rotated about

the Z axis and have the same equations with opposite angles of rotations. The transformation for the north and south lamp is shown here

$$\begin{aligned}
 x &= (x - 2 * x_c) \cos(\theta) + z \sin(\theta) + 2 * x_c \cos(\theta) \\
 y &= y \\
 z &= z \cos(\theta) - (x - 2 * x_c) * \sin(\theta) \\
 m &= m \cos(\theta) + o \sin(\theta) \\
 n &= n \\
 o &= o \cos(\theta) - m \sin(\theta)
 \end{aligned}
 \tag{4.1}$$

The transformation for the east and west lamp is shown here

$$\begin{aligned}
 x &= (x - 2 * x_c) \cos(\theta) + y \sin(\theta) + 2 * x_c \cos(\theta) \\
 y &= y \cos(\theta) - (x - 2 * x_c) * \sin(\theta) \\
 z &= z \\
 m &= m \cos(\theta) + n \sin(\theta) \\
 n &= n \cos(\theta) - m \sin(\theta) \\
 o &= o
 \end{aligned}
 \tag{4.2}$$

There are three different configurations the simulator was looked at. Figure 5.7 shows the first configuration.

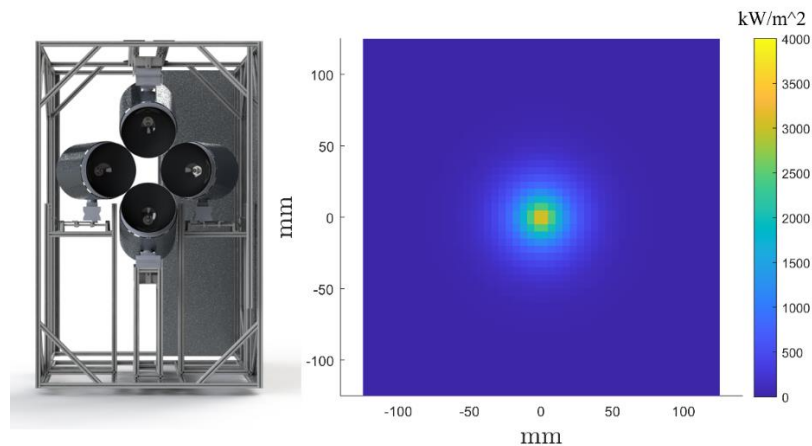


Figure 5.7: First lamp configuration and flux map; The lamps are set at an inclination angle of 24.5 degrees

This configuration has a peak flux of around 4000 suns and 3.29kW of radiative power in a 60mm-diameter aperture. The next configuration is shown in figure 5.8.

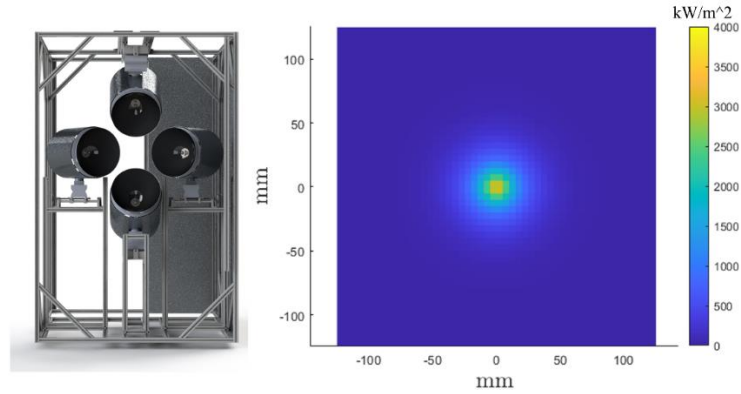


Figure 5.8: second lamp configuration and flux map; The lamps are set at an inclination angle of 27.8 degrees

This configuration also has a peak flux of around 4000 suns and 3.24kW of radiative power in a 60mm-diameter aperture. This configuration was made to make room for the fifth lamp of the simulator to be added. The small decrease in power is well worth the added bonus of the xenon lamp as shown in figure 5.9.

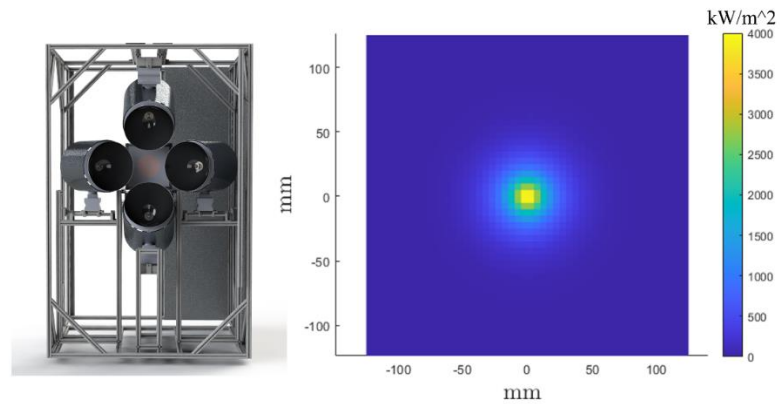


Figure 5.9: Third lamp configuration and flux map; The lamps are set at an inclination angle of 27.8 degrees with the added xenon lamp

The final MCRT flux map of the 5-lamp simulator with a finer mesh is shown below in figure 5.10.

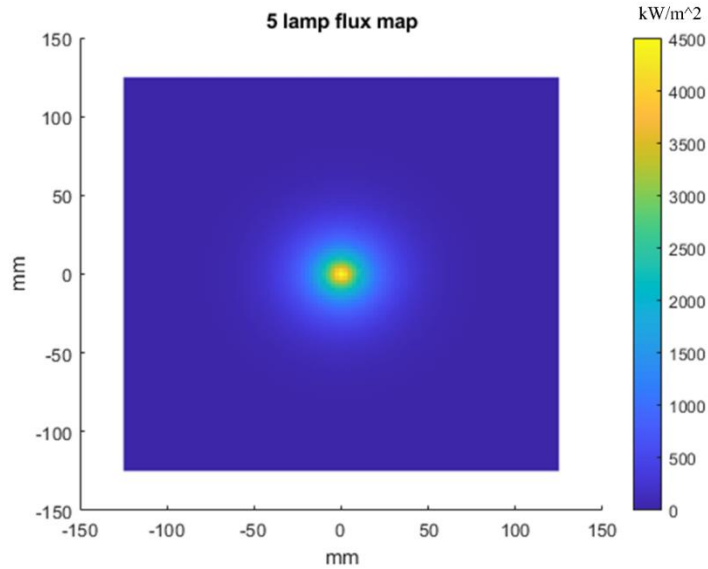


Figure 5.10: Flux map of full 5 lamp simulator; The color bar on the right shows flux in kW/m² and has a peak flux of 4509; The total power in the 60mm aperture is 3.6839kW

The reason this plot is different from the one shown in 5.9 is because the mesh is finer. The rays are sorted into smaller areas so the flux can be calculated more accurately.

Figure 5.11 shows the effect of moving the flux target to different locations.

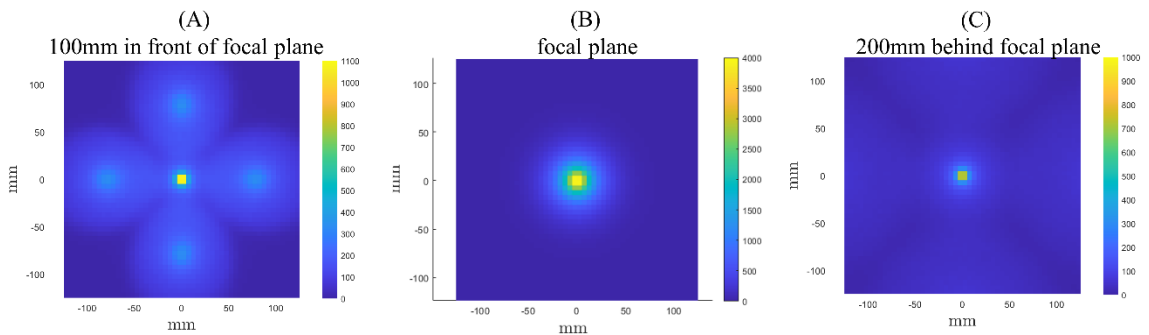


Figure 5.11: Flux maps at different positions in front and behind the focal plane

When the focal plane is moved to different positions the flux on the target changes noticeably. It is important to note that whether the flux is 100mm in front or 100mm behind the shape of the flux will stay the same but the intensity will be lower.

CHAPTER VII

CONCLUSION AND FUTURE WORKS

This paper showed the design, modeling, and modeling results of a novel high flux solar simulator. This simulator is unique because it features two different lamp types, two different reflector types, and the ability to change the flux aperture with the central xenon lamp. In the future the simulator characterization will be completed with the use of a Lambertian target and calorimeter. More studies will also be done to see the effect of arc models on the impact of the simulator.

REFERENCES

1. Schrader AJ, De Dominicis G, Schieber GL, et al. Solar electricity via an Air Brayton cycle with an integrated two-step thermochemical cycle for heat storage based on Co₃O₄/CoO redox reactions III: Solar thermochemical reactor design and modeling. *Solar Energy* 2017;150(584-595, doi:<https://doi.org/10.1016/j.solener.2017.05.003>
2. Tawfik M, Tonnellier X, Sansom C. Light source selection for a solar simulator for thermal applications: A review. *Renewable and Sustainable Energy Reviews* 2018;90(802-813, doi:<https://doi.org/10.1016/j.rser.2018.03.059>
3. Wang W, Aichmayer L, Garrido J, et al. Development of a Fresnel lens based high-flux solar simulator. *Solar Energy* 2017;144(436-444, doi:<https://doi.org/10.1016/j.solener.2017.01.050>
4. Schrader AJ, Schieber GL, Ambrosini A, et al. Experimental demonstration of a 5 kWth granular-flow reactor for solar thermochemical energy storage with aluminum-doped calcium manganite particles. *Applied Thermal Engineering* 2020;173(115257, doi:<https://doi.org/10.1016/j.applthermaleng.2020.115257>
5. Gallo A, Marzo A, Fuentealba E, et al. High flux solar simulators for concentrated solar thermal research: A review. *Renewable and Sustainable Energy Reviews* 2017;77(1385-1402, doi:<https://doi.org/10.1016/j.rser.2017.01.056>
6. Ji Y, Cook MJ, Hanby VI, et al. CFD modelling of double-skin facades with venetian blinds. *Building Simulation* 2007 2007;1491-1498
7. Levêque G, Bader R, Lipiński W, et al. Experimental and numerical characterization of a new 45 kWel multisource high-flux solar simulator. *Optics Express* 2016;24(22):A1360-A1373, doi:10.1364/OE.24.0A1360
8. Li X, Chen J, Lipiński W, et al. A 28 kWel multi-source high-flux solar simulator: Design, characterization, and modeling. *Solar Energy* 2020;211(569-583, doi:<https://doi.org/10.1016/j.solener.2020.09.089>
9. Shankar R, Shim WJ, An JG, et al. A practical review on photooxidation of crude oil: Laboratory lamp setup and factors affecting it. *Water Research* 2015;68(304-315, doi:<https://doi.org/10.1016/j.watres.2014.10.012>
10. Siegel NP, Roba JP. Design, Modeling, and Characterization of a 10 kWel Metal Halide High Flux Solar Simulator. *Journal of Solar Energy Engineering* 2018;140(4), doi:10.1115/1.4039658
11. Modest MF. Radiative Heat Transfer. Academic Press: United States of America; 2003.
12. Mikš A, Novák P. Determination of unit normal vectors of aspherical surfaces given unit directional vectors of incoming and outgoing rays: comment. *Journal of the Optical Society of America A* 2012;29(7):1356-1357, doi:10.1364/JOSAA.29.001356

13. Mahan JR. The Monte Carlo Ray-Trace Method in Radiation Heat Transfer and Applied Optics. ASME Press: 2019.
14. Roba JP, Siegel NP. The design of metal halide-based high flux solar simulators: Optical model development and empirical validation. Solar Energy 2017;157(818-826, doi:<https://doi.org/10.1016/j.solener.2017.08.072>